IN-PLANE MECHANICAL PROPERTIES OF DUCTILE COMPOSITES WITH UNIDIRECTIONAL STAINLESS STEEL FIBRE REINFORCED LAYERS

K. Allaer[a,b], I. De Baere[a], W. Van Paepegem[a] and J. Degrieck[a]

[a] *Department of Materials Science and Engineering, Faculty of Engineering and Architecture, Ghent University, Technologiepark 903, B-9052 Zwijnaarde, Belgium.*
[b] *SIM program NanoForce, Technologiepark 935, B-9052 Zwijnaarde, Belgium.*
E-mail: Klaas.Allaer@UGent.be, Tel. +32 9 331 04 23

Keywords: Stainless steel fibre, Mechanical properties, Stress/strain curves, Fractography

Abstract
Innovative continuous stainless steel fibre filaments with a 30µm diameter allow the production of ductile composite laminates exhibiting high strain-to-failure behaviour. This study introduces unidirectional stainless steel fibre reinforced epoxy composites and reports the mechanical behaviour under quasi-static tension and compression in both principle material directions, along with the in-plane shear properties. In-plane mechanical properties, including elastic moduli and strengths were determined by use of resistance strain gauge measurements and Digital Image Correlation (DIC) technique, providing full field strain maps during loading and identifying local strain concentrations. The damage morphology of failed specimens loaded in different directions was examined using both optical microscopy and Scanning Electron Microscopy (SEM), identifying the principle features of failure.

1. Introduction

Conventional fibre materials such as carbon and glass fibres have been known to be the first choice of reinforcing materials, owing their success to high specific strength and stiffness, facilitating the development of high-performance lightweight structures [1,2]. However these fibrous materials tend to fail in a brittle manner, exhibiting low failure strains and deformation capabilities. A new ductile stainless steel fibrous layer was developed by NV Bekaert SA, consisting of continuous fibre filaments with a 30 µm diameter, which can be bundled and woven into any textile fabric architecture. The inherent ductility and toughness properties of steel reinforcing materials, combined with its high stiffness allow for high strain-to-failure composite materials.

Steel as a reinforcing material has been used in many applications, some of which are reinforced concrete and external reinforcements of constructions [3], flexible transmission belts [4] and radial tires [5]. The latter two incorporate steel cords and steel wires having diameters ranging from 0.1 mm up to several millimeters, whereas the diameter of fibres varies from 5 µm to 50 µm. Injection molded parts with steel cords embedded in a glass fibre thermoplastic composite are commercially available for energy absorption applications [6]. At present, steel fibre materials found their way in filtration application [7] and electromagnetic interference (EMI) shielding [8]. To the authors' knowledge, very little work has been done concerning the use continuous stainless steel fibres as a reinforcing material, embedded in a polymeric matrix system, for use in structural composite applications. Within the same research project, Callens et al. [9] have investigated the same stainless steel fibre reinforcement material imbedded in a brittle epoxy and thermoplastic polyamide matrix.

In this study continuous stainless steel fibrous layers were imbedded into a more ductile epoxy system. The in-plane mechanical behaviour was investigated experimentally by means of quasi-static tensile and compression tests in both principle material directions, together with in-plane shear tests. Digital Image Correlation technique (DIC) was used to map full field surface strains and local strain concentrations. Fractographic analysis of the failed specimen was conducted using optical microscopy and Scanning Electron Microscopy (SEM). The basic mechanical and specific mechanical properties for the unidirectional stainless steel fibrous ductile composite were compared to the experimental results obtained by Callens et al. [9] as well as with a commercial unidirectional E-glass fibre epoxy and monolithic steel grades.

2. **Materials and methods**

2.1. Unidirectional stainless steel composite material

Annealed AISI 316L stainless steel continuous fibres with a filament diameter of 30 μm were supplied by NV Bekaert SA and used as reinforcing material embedded in a ductile epoxy resin system EPIKOTE™ Resin MGS RIM 135. The fibres were bundled into yarns consisting of 275 filaments and woven in a quasi-unidirectional fabric having a dry areal weight of 1425 g/m^2. The composite laminates were fabricated using the Vacuum Assisted Resin Transfer Molding (VA-RTM) technique and subsequently cured in an electrically heated oven at 80 °C for 15 h in accordance to the standard curing cycle recommended by the manufacturer. The fibre volume fraction of the steel fibre composite laminate was determined in accordance to ASTM D 792-08 and was found to have an average value of 42.3 %.

2.2. Experimental testing

Unidirectional (UD) specimens used for the tensile and compression tests were cut from eight-ply $[0]_8$ laminates and had a nominal thickness of 3.0 mm. The specimens used to determine the in-plane shear properties were cut from $[0/90]_{2s}$ cross-ply laminates at a 45° angle to give specimens with a $[+45/-45]_{2s}$ stacking sequence. The coupons were bonded with beveled aluminum end tabs to prevent slipping in the tensile machine grips and local failure at the loading points. All experimental tests were performed at room temperature on a 100 kN servo-hydraulic INSTRON 8801 testing machine equipped with an AlignPRO alignment fixture. The quasi-static tests were displacement-controlled with a crosshead speed of 2 mm/min. Strain gauges with a resistance of 350 Ω were bonded to the back side of the specimens to monitor the axial and transverse strain.

The stereovision or 3D Digital Image Correlation (3D-DIC) method was used for measuring the full-field displacements and deformations at the materials' surface. The method is based on pairs of digital images, where a deformed image from every loading step is compared with the undeformed reference image taken prior to loading [10]. The two camera stereovision setup was chosen because of the ability to capture out-of-plane displacements and the flexibility in terms of positioning and alignment of the optical system with regard to the specimen surface. By calibrating the camera system, intrinsic and extrinsic parameters are taken into account during the image correlation process, ensuring accurate strain results. A random speckle pattern was applied on the specimen surface and monitored with 2 mega-pixel 8-bit CCD AVT Stingray F-201 B 1/1.8" cameras throughout the loading event. During quasi-static loading, images with a 1624 x 1232 pixel resolution were acquired at a sampling rate of 2 Hz and synchronized with the load-displacement signals from the tensile machine. In order to determine the specimen surface displacement field and subsequent calculation of the strain contours, a correlation between these paired images was calculated using the MatchID

software [11]. Results from the digital image correlation have been compared with resistance strain gauge measurements to validate the method. At least 5 specimens were tested for each experimental setup and a statistical analysis of the data listed the mean values and standard deviations for each type of test.

3. Results and discussion

3.1. Tensile, compressive and shear performance of UD steel fibre/epoxy laminates

Fig. 1 shows the in-plane stress-strain behaviour of UD steel fibre/epoxy specimens tested under tensile, compression and shear loading conditions. The axial tensile response (Fig. 1.1a) shows a clear nonlinear response with an initial elastic part up to approximately 0.15 % strain. Following the linear deformation, the composite material starts to yield when the elastic limit of the material is reached. Following this yield point, the material continues to carry increasing tensile stresses, reaching an average ultimate tensile strength of 311.6 MPa and a failure strain up to 19.15 %. Fig. 1.1b shows a longitudinal strain contour at the yielding section of the stress-strain curve illustrating the strain concentration around the PET binder yarns. The uniaxial tensile response of the composite tends to exhibit the same elastic-plastic behaviour as the 316L stainless steel fibre filament. It is clear that the full strain potential of the ductile stainless steel fibres is retained in the composite material behaviour. In the transverse direction (Fig. 1.1c), the composite experiences mainly elastic deformation before failure, an average transverse failure strain of 0.31% is reported. Transverse failure of a UD composite is mainly dominated by the matrix properties and state of stress at the fibre/matrix interface.

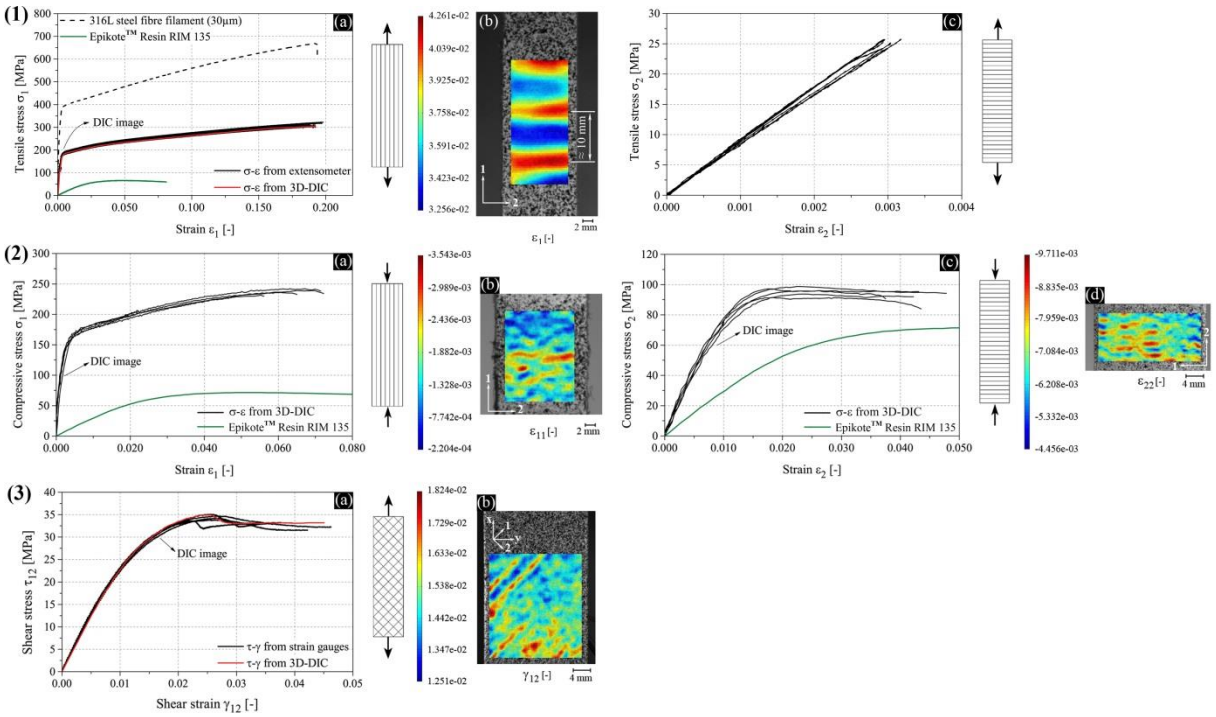

Figure 1. In-plane stress-strain response of UD stainless steel fibre/epoxy composite: (1) tension of $[0]_8$ and $[90]_8$ specimens, fibre filament and neat epoxy resin, (2) compression of $[0]_8$ and $[90]_8$ specimens, (3) shear response of $[+45/-45]_{2s}$ specimens.

The lower transverse strength is partially due to the low normal interfacial strength of the 316L stainless steel fibres and the epoxy polymer.

Fig. 1.2 shows the compressive response of UD steel fibre/epoxy laminates, and ductile neat epoxy resin. In the case of longitudinal compression (Fig. 1.2a), the material exhibits a linear elastic stress-strain relation up to approximately 0.16 % strain, after which a transit to nonlinear behaviour is observed. As the compressive strain reaches a magnitude of 0.34 %, a distinct yield region is noticed, further compressive loading ultimately leads to a gradually decreasing tangent modulus. Fig. 1.2b illustrates the full-field strain contour at the point of non-linearity during axial compressive loading. A local strain concentration across the width of the gauge section is noticed. This presumably corresponds with the onset of fibre microbuckling and kink band formation which is the failure mode encountered in longitudinal compression of this material. In the case of transverse compression (Fig. 1.2c), the onset of nonlinear behaviour lies at a relatively higher applied strain (0.7%) compared to the 0° specimens. When a compressive strain of 1.6% is reached, the stress-strain response tends towards an apparent uniform stress. Values for this plateau of constant stress are recorded as the compressive strength. Fig. 1.2d shows the full-field strain contour at the point of non-linearity during the transverse compressive loading. It is observed that at the end of the linear behaviour, compressive strain concentration lines develop in the transverse direction, corresponding to the fibre bundles lying along that 90° path.

Fig.1.3a shows the relation between the shear stress and strain, illustrating linear material response up to approximately 0.6% shear strain, followed by nonlinear behaviour. As the level of stress is increased, a peak shear stress is reached, followed by a softening process which results in a uniform stress plateau. Fig. 1.3b shows the full-field strain contour at 0.15% shear strain, illustrating the heteregeneous strain field and local shear band concentrations at the nonlinear region of the shear stress-strain curve.

The in-plane mechanical properties of the UD stainless steel fibre/epoxy composite reported in this paper are summarized in Table 1. In this table, subscripts 1 and 2 refer to the fibre direction and the transverse direction, respectively.

Tensile properties	Magnitude
Longitudinal modulus, E_{11t} (GPa)	82.5 ± 4.8
Transverse modulus, E_{22t} (GPa)	8.9 ± 0.4
Major Poisson's ratio, ν_{12}	0.338 ± 0.015
Offset yield strength $\sigma_{Y,0.1\%}$ (MPa)	174.4 ± 5.6
Longitudinal tensile strength, X_{11t} (MPa)	311.6 ± 9.0
Transverse tensile strength, Y_{22t} (MPa)	25.9 ± 0.9
Offset yield strain $\varepsilon_{Y,0.1\%}$ (%)	0.34 ± 0.01
Longitudinal failure strain, ε_{11c}^{f} (%)	19.15 ± 0.52
Transverse failure strain, ε_{22c}^{f} (%)	0.312 ± 0.014

Compressive properties	Magnitude
Longitudinal compressive modulus, E_{11c} (GPa)	62.1 ± 1.6
Transverse compressive modulus, E_{22c} (GPa)	8.7 ± 0.7
Longitudinal compressive strength, X_{11c} (MPa)	239.3 ± 12.5
Transverse compressive strength, Y_{22c} (MPa)	95.4 ± 2.9
Longitudinal failure strain, ε_{11c}^{f} (%)	6.73 ± 0.67
Transverse failure strain, ε_{22c}^{f} (%)	2.10 ± 0.26
Shear properties	
Shear modulus, G_{12} (GPa)	2.63 ± 0.07
Shear yield stress, $\tau_{12,Y}$ (MPa)	15.1 ± 0.2
Shear strain at yield, $\gamma_{12,Y}$ (%)	0.62 ± 0.02
Shear strength, S_{12}^{ult} (MPa)	34.3 ± 0.6
Shear strain at shear strength, γ_{12}^{ult} (%)	2.59 ± 0.12

Table 1. In-plane mechanical properties of unidirectional stainless steel fibre/epoxy composite.

In order to compare the performance to that of other materials, mechanical and specific mechanical properties of the unidirectional stainless steel ductile composites are summarized in Table 2, together with those of other material grades. Using a more brittle epoxy or thermoplastic system shows lower values for the specific modulus and specific strength. The longitudinal stiffness of the stainless steel composite is higher than that of commercial unidirectional E-glass/epoxy, but due to the lower density the specific strength is considerable higher. Comparing to monolithic steel grades, the specific modulus is slightly higher than that of the stainless steel composite, while the specific strength of plain carbon steel returns a much lower value. When strength is a critical design parameter, the choice of conventional fibrous materials such as glass and carbon is more beneficial. However, these materials

exhibit linear behaviour with relatively low failure strains and tend to fail in a brittle manner, making these materials susceptible to dynamic loading events.

Material	V_f (%)	ρ (kg/m³)	E (GPa)	σ (MPa)	$\varepsilon_{failure}$ (-)	E/ρ (GPa/g/cm³)	σ/ρ (MPa/g/cm³)
UD stainless steel fibre / ductile epoxy	42	3936	82,5	315	19.15	21,0	80,0
UD stainless steel fibre / brittle epoxy [a]	44	4187	67.0	259.6	7.3	16.0	62.0
UD stainless steel fibre / polyamide 6 [a]	41	4000	73.2	265.6	12.7	18.3	66.4
Commercial E-glass/epoxy [b]	55	2100	39	1080	2.8	18,6	514,3
Stainless steel (AISI 316L)	-	7990	193	667	19.5	24,2	83,5
Carbon steel (AISI 1025) [b]	-	7800	207	394	25.0	26,5	50,5

[a] Callens et al. [9], [b] Daniel et al. [12]

Table 2. Mechanical and specific mechanical properties of unidirectional stainless steel fibre polymer composite laminates compared to other materials.

Hybridization of conventional reinforcing materials with stainless steel fibrous layers could enable the tailoring of composite materials by combining the advantages of different fibres. Incorporating these high strain-to-failure fibrous layers in conventional fibre materials would result in hybrid composites combining high structural performance and plastic deformation capability, addressing the unique ductile features encountered in these materials. These stainless steel fibres can be woven into any textile architecture, giving considerable design freedom and the ability of using conventional composite manufacturing processes. The drapability properties of the fabrics allows for designing more complex geometries and local ductile reinforcements in a structure or component which can be directly embedded in the composite ply stacking.

3.2. Prediction of elastic properties

Various analytical micromechanical models have been developed for predicting composite engineering constants. These models are based on the elastic properties of the constituent materials and the morphology of the composite, such as fibre volume fraction and geometric packing parameters. Using the semi-empirical model presented by Halpin and Tsai [13] the elastic properties of the UD lamina were calculated using the set of equations (1-4) presented in Table 2. Indices *f* and *m* are referring to fibre and matrix, respectively. The expressions for the longitudinal modulus and the Possion's ratio reduce to the same form as the rule of mixture (ROM) equations. Parameter ξ is a measure depending on the fibre cross-section and packing geometry. The value of ξ is set equal to 2 for non-circular cross-section fibres in a diamond-array packing. The results of the predicted elastic constants are shown in Table 3.

Properties	Equations	Eq.	Calculated	Experimental
E_{11} (GPa)	$E_{11} = E_f V_f + E_m V_m$	(1)	83.21	82.5 ± 4.8
E_{22} (GPa)	$E_{22} = E_m \frac{1+\xi\,\eta\,V_f}{1-\eta\,V_f}$ where $\eta = \frac{E_f - E_m}{E_f + \xi E_m}$ and $\xi = 2$	(2)	8.32	8.9 ± 0.4
G_{12} (GPa)	$G_{12} = G_m \left[\frac{(G_{12f} + G_m) + V_f (G_{12f} - G_m)}{(G_{12f} + G_m) - V_f (G_{12f} - G_m)} \right]$	(3)	2.39	2.63 ± 0.07
υ_{12}	$\upsilon_{12} = V_f\, \upsilon_{12f} + V_m\, \upsilon_m$	(4)	0.34	0.338 ± 0.015

Table 3. Calculated and experimental in-plane elastic properties for UD stainless steel fibre epoxy lamina.

Although the given expressions only form an approximate representation, it was found that the analytical results are in good agreement with the experimental values.

3.3. Fractographic analysis of failed surfaces

The morphology of the fractured surfaces of unidirectional steel fibre/epoxy laminates has been examined to identify the characteristic failure features for the applied loading modes.
Fig. 2 shows the tensile failure of UD steel fibre/epoxy composite material. Damage initiated consequently at the PET binder yarns, DIC strain maps showed local strain concentrations at these binder yarns during tensile loading (Fig. 1.1b). A fibre bundle misalignment at the binder crossover point is shown in Fig. 2b. This undulation results in an out-of-plane waviness in the 1-3 plane. Initially undulated fibre bundles tend to straighten during tensile testing, causing stress concentration zones in the region of the binder yarns.
Microscopic in-situ monitoring (Fig. 2c) showed that matrix microcracks initiate parallel to these PET yarns at about 0.15 % applied strain, corresponding to the yield strain of the fibres. These microcracks propagate along the binder yarn, perpendicular to the loading direction, and initiate fibre/matrix debonding at the interface (Fig. 2d).

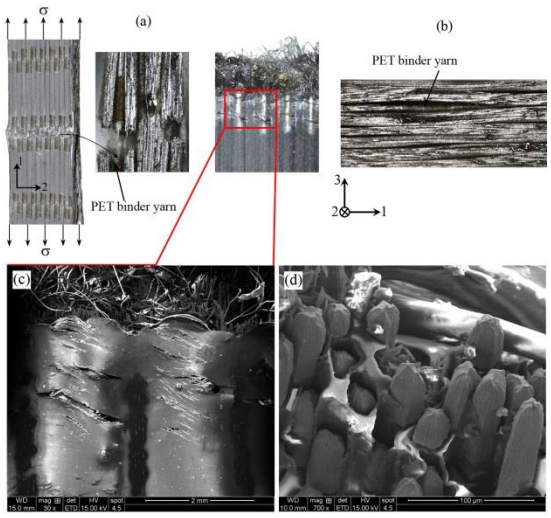

Figure 2. Tensile fracture of $[0]_8$ UD stainless steel fibre/epoxy composite: (a-b) edge view of $[0]_8$ specimens, (c) local matrix cracks, (d) plastic necking of fibres.

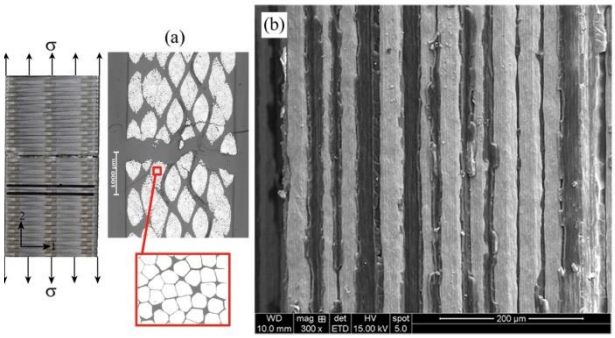

Figure 3. Tensile fracture of $[90]_8$ UD stainless steel fibre/epoxy composite: (a) edge view of $[90]_8$ specimens, (b) identification of zero matrix rest fractions.

The strain concentration resulting from this interfacial failure together with reaching the yield strain fibres, initiates plastic deformation, leading to fibre necking and decreasing of the fibre cross-section. Even after cracking of the matrix and fibre yielding, the laminate continues to carry increasing tensile stresses. During the plastic deformation, matrix crack density and fibre/matrix debonding increases, prohibiting deformational stress in the matrix to be transferred to the fibres. Successive damage development and fibre plastic straining ultimately leads to catastrophic failure of the laminate.

Fig. 3a shows an edge view of a failed transverse loaded specimen with a detailed view of the fibre bundle packing. Failure of transverse tensile loaded coupons is strongly controlled by the matrix properties and normal fibre/matrix interfacial strength As a result of the irregular hexagonal cross sections of the fibres, a region of highly intensified strain is induced at these points, leading to plastic deformation of the matrix with fibre/matrix debonding and interfacial failure. Evidence of this low normal interfacial strength is shown in Fig. 3b, showing no epoxy rest fractions on the steel fibre surfaces.

Fig. 4 shows the compression fracture modes of UD steel fibre/epoxy specimens tested in both axial and transverse direction. Under axial compression, a localized failure zone is noticed, associated with microbuckling or kink-band formation of the fibres (Fig. 4a). The

elastic instability of the initial misaligned fibres promotes the microbuckling mode, enabling the simultaneous rotation of the fibres. During rotation of the fibres, high shear stresses develop at the fibre/matrix bond which can lead to interfacial failure. However, examining the fracture morphology did not reveal any presence of fibre/matrix debonding or ply delaminations. It is presumed that the tough epoxy system provides lateral support during plastic yielding and kink-band formation of the fibres. Transverse compression is mainly influenced by the matrix compressive properties and fibre/matrix interface. High compressive stress concentrations at the interface cause localized yielding in the matrix, initiating shear failure. Fig. 4b illustrates the formation of shear cusps or hackles during transverse compression. These localized cracks propagate in the matrix and fibre bundles, leading to an overall shear failure mode along a fracture plane angle $\alpha \approx 42° - 44°$ with the loading direction (Fig. 4c).

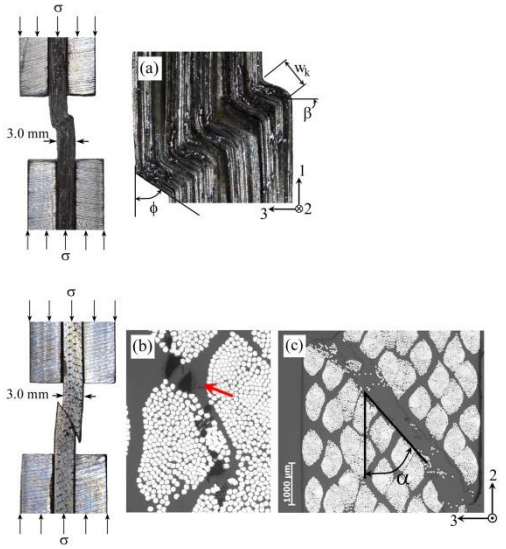

Figure 4. Compression fracture of $[0]_8$ and $[90]_8$ UD stainless steel fibre/epoxy composite: (a) edge view of axial compressive failure mode with kink band formation, (b-c) identification of matrix shear failure during transverse compression.

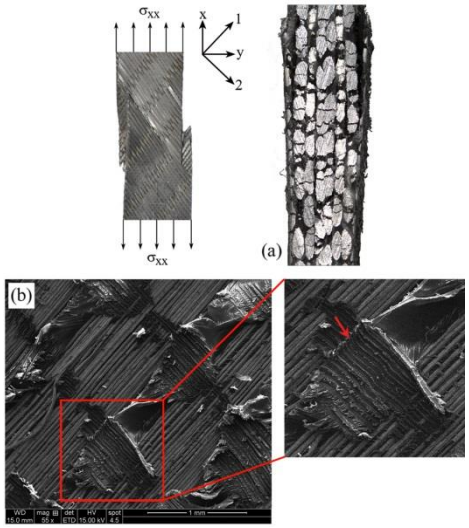

Figure 5. Shear fracture of $[+45/-45]_{2s}$ UD stainless steel fibre/epoxy composite (a) macroscopic edge view showing bundle splitting and delaminations, (b) top view showing shear failure mode.

The shear failure surface of unidirectional steel fibre/epoxy composite material is shown in Fig. 5. As a result of the low fibre/matrix interfacial strength, interlaminar cracks develop between the plies and fibre bundles. Debonding between the layers along with fibre bundle splitting (Fig. 5a) promotes the rotation or scissoring of the fibres ultimately leading to delamination and interlaminar shearing over the entire specimen. Further loading of the material increases the rotation of the fibre bundles towards the loading axis, resulting in shear dominated failure of the epoxy between adjacent fibre bundles. Fig. 5b also shows smooth fibres with no matrix rest fraction implying low interfacial strength at the fibre/matrix bond.

4. Conclusion

The longitudinal tensile results show that the full tensile strain capacity of the ductile stainless steel fibres is retained in the composite up to laminate failure. On the other hand, transverse tension exhibits low failure stress and strain. Fracture surfaces show no presence of matrix rest fractions on the fibres, which indicate a relatively low fibre/matrix interfacial strength. The specific mechanical properties of this composite material are comparable to those reported for a commercial unidirectional E-glass/epoxy and monolithic stainless and carbon

steel grades. In-plane elastic and strength properties were higher compared to using a more brittle epoxy matrix or thermoplastic polyamide 6 polymer. A general agreement was found between the calculated elastic properties using the micromechanical approach and the experimental values. Longitudinal compressive behaviour is mainly dominated by the out-of-plane fibre waviness enabling fibre microbuckling and kink-band formation, whereas in transverse compression, high compressive stress concentrations at the interface cause the matrix to shear and debond from the fibres, leading to an overall shear failure mode. In-plane shear failure is dominated by the fibre/matrix interfacial strength and matrix properties. Shear deformation triggers fracture by debonding between the fibres and epoxy and the formation of epoxy shear bands between adjacent fibre bundles, resulting in ply delamination. Failure surfaces show evidence of low fibre/matrix interfacial strength. Fibre/matrix interfacial strength has a great influence on the overall mechanical properties of the steel fibre/epoxy laminate. Improving this interfacial strength by chemical surface modification of the fibres could enhance the mechanical properties. Further research concerns the application of an optimized treatment and influence on static and dynamic material properties.

Acknowledgements

This research was supported by SIM-Flanders and conducted in the framework of the SIM Nanoforce program (Next generation nano-engineered polymer-steel/CNT hybrids) through the NaPoS project. The authors wish to thank NV Bekaert SA for support and the supply of the steel fibre quasi-UD reinforcing material used in this study.

References

[1] P. Delhaès. Fibers and Composites. Taylor & Francis, 2003.
[2] A. Baker, S. Dutton, S. Kelly. Composites Materials for Aircraft Structures: Second Edition. American Institute of Aeronautics and Astronautics, 2004.
[3] A. Lopez, N. Galati, Alkhadraji, A. Nanni. Strengthening of a reinforced concrete bridge with externally bonded steel reinforced polymer (SRP). Composites Part B: Engineering, 38(4):429-36, 2007.
[4] T. Akasaka, K. Kabe, K. Sako. Bending stiffness of a tire-belt structure with steel cords. Composites Science and Technology, 24:215-30, 1985.
[5] R. Rajan, P. Volpin, L. Zingales. The eclipse of the U.S. tire industry. University of Chicago Press, 2000.
[6] A. Radtke, V. Van Wassenhove, K. Van Koert, F. Vöge, D. Moors, O. Geiger, D. Fertig. AISI-Component: Reinforcing with Steel Cord. Kunstoffe international, 11:67-71, 2012.
[7] Bekaert Advanced Filtration Literature.
[8] S. Wen, DDL. Chung. Electromagnetic interference shielding reaching 70 dB in steel fiber cement. Cement and Concrete Research, 34:329-332, 2004.
[9] MG. Callens, L. Gorbatikh, I. Verpoest. Ductile steel fibre composites with brittle and ductile matrices. Composites Part A: Applied Science and Manufacturing, 2014.
[10] MA. Sutton, JJ. Orteu, HW. Schreier. Image correlation for shape, motion and deformation measurements. New York: Springer, 2009.
[11] MatchID software. <http://www.macthid.org/>.
[12] IM. Daniel, O. Ishai. Engineering mechanics of composite materials. New York: Oxford University Press, 1994.
[13] JC. Halpin, JL. Kardos. The Halpin-Tsai Equations: A Review. Polymer Engineering and Science, 16(5):970-80, 1976.